Systematic analysis of the MAPK signaling network reveals MAP3K-driven control of cell fate

Highlights

- Comprehensive study provides an in-depth map of MAPK connectivity and cross-regulation
- MAP3Ks are uniquely poised to regulate cell fate by combinatorial pathway activation
- Identification of synergistic, paradoxical functions of ERK/
 JNK dual activation
- When combined with ERK, JNK activation promotes cellcycle entry rather than apoptosis

Authors

Amy F. Peterson, Kayla Ingram, E.J. Huang, Jeeun Parksong, Connor McKenney, Gabriel S. Bever, Sergi Regot

Correspondence

sregot@jhmi.edu

In brief

Peterson et al. perform a comprehensive analysis of MAPK perturbations in live single cells. They identify MAP3K specificity as a primary node of cell behavior control as MAP3Ks integrate information from upstream stimuli to unique combinations of downstream MAPK activity. This identifies combinatorial pathway activation as the mechanism that controls the paradoxical role of JNK in pro-proliferation or proapoptosis.







Article

Systematic analysis of the MAPK signaling network reveals MAP3K-driven control of cell fate

Amy F. Peterson,^{1,2,3} Kayla Ingram,^{1,2,3} E.J. Huang,⁴ Jeeun Parksong,^{1,2,3} Connor McKenney,^{1,2,3} Gabriel S. Bever,^{4,5} and Sergi Regot^{1,2,3,6,*}

¹Department of Molecular Biology and Genetics, The Johns Hopkins University School of Medicine, Baltimore, MD, USA

*Correspondence: sregot@jhmi.edu https://doi.org/10.1016/j.cels.2022.10.003

SUMMARY

The classic network of mitogen-activated protein kinases (MAPKs) is highly interconnected and controls a diverse array of biological processes. In multicellular eukaryotes, the MAPKs ERK, JNK, and p38 control opposing cell behaviors but are often activated simultaneously, raising questions about how input-output specificity is achieved. Here, we use multiplexed MAPK activity biosensors to investigate how cell fate control emerges from the connectivity and dynamics of the MAPK network. Through chemical and genetic perturbation, we systematically explore the outputs and functions of all the MAP3 kinases encoded in the human genome and show that MAP3Ks control cell fate by triggering unique combinations of MAPK activity. We show that these MAPK activity combinations explain the paradoxical dual role of JNK signaling as proapoptotic or pro-proliferative kinase. Overall, our integrative analysis indicates that the MAPK network operates as a unit to control cell fate and shifts the focus from MAPKs to MAP3Ks to better understand signaling-mediated control of cell fate.

INTRODUCTION

Mitogen-activated protein kinases (MAPKs) are essential signaling proteins present in all major eukaryotic lineages (Suga et al., 2014). MAPK pathways involve a classic three-tiered kinase cascade where a MAP3K phosphorylates and activates a MAP2K, which in turn phosphorylates and activates a MAPK (Kyriakis and Avruch, 2012). Once active, MAPKs control critical cellular decisions, from mating or osmoregulation in budding yeast to proliferation, differentiation, and apoptosis in multicellular eukaryotes, and they have thus been implicated in many diseases ranging from cancer to immune disorders and neuropathies (Arthur and Ley, 2013; Dhillon et al., 2007; Johnson and Lapadat, 2002; Wagner and Nebreda, 2009). Remarkably, MAPKs are conserved throughout eukaryotes to the point that human MAPKs can functionally complement yeast mutant strains (Galcheva-Gargova et al., 1994; Han et al., 1994). In mammalian cells, a broad diversity of inputs control MAPK signaling, from growth factors and cytokines (Arthur and Ley, 2013; McCubrey et al., 2007) to ribosome collisions or environmental stress (Saitoh et al., 1998; Wu et al., 2020), and at the same time, MAPKs control a wide range of responses in different contexts, raising the long-standing question of how input-output specificity is achieved.

In humans, the MAPK signaling network is composed of 24 MAP3Ks that control 7 MAP2Ks which in turn control 14 MAPKs (Manning et al., 2002). Among the 14 MAPKs, three major groups are identified based on their sequence homology, functional redundancy, and shared activation mechanisms: the extracellular signal-related kinases (ERKs) (ERK1/2), the p38s $(\alpha, \beta, \delta, \gamma)$, and the c-Jun N-terminal kinases (JNKs) (1/2/3). ERK signaling is typically associated with control of proliferation, survival, and differentiation, whereas JNK and p38, also known as stress activated protein kinases (SAPKs), are associated with cell-cycle arrest and apoptosis (Kyriakis and Avruch, 2012). However, these functional roles are often context dependent. For example, JNK activity can promote either proliferation or apoptosis in different contexts (La Marca and Richardson, 2020; Tournier, 2013). This dual functional role of JNK activity has been recognized in Drosophila and mouse models, and several hypotheses have been proposed, including the existence of dynamics-dependent functions of JNK (i.e., sustained versus transient JNK signaling) (Ventura et al., 2006). In fact, the temporal patterns of ERK activity also trigger opposed cellular behaviors (i.e., proliferation versus cell-cycle arrest) (Aikin et al., 2020). Together, these studies highlight the need for single-cell approaches to monitor MAPK activity with high temporal resolution.



²Department of Oncology, The Johns Hopkins University School of Medicine, Baltimore, MD, USA

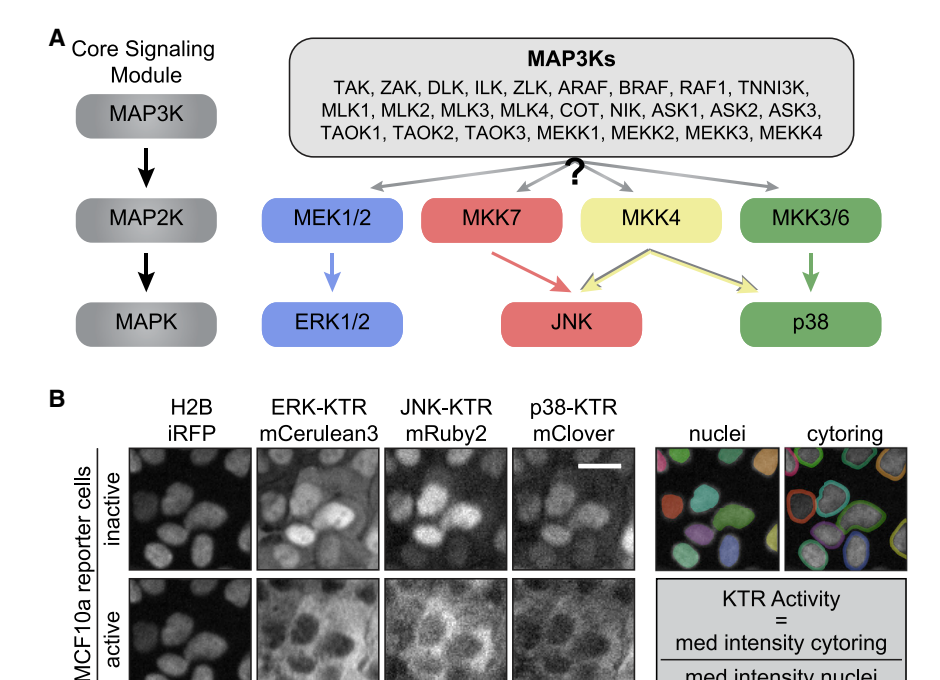
³The Biochemistry, Cellular, and Molecular Biology Graduate Program, The Johns Hopkins University School of Medicine, Baltimore, MD, USA

⁴Center for Functional Anatomy & Evolution, The Johns Hopkins University School of Medicine, Baltimore, MD, USA

⁵Department of Medicine, Division of Cardiology, The Johns Hopkins University School of Medicine, Baltimore, MD, USA

⁶Lead contact





MAPK pathways are often depicted as linear cascades, vet numerous studies have shown a high degree of cross talk and feedback regulation between and within MAPK pathways, suggesting that the system operates as a network (Fey et al., 2012; Heinrichsdorff et al., 2008; Miura et al., 2018). While the connectivity between MAP2Ks and MAPKs is well stablished (Figure 1A), the MAP3K to MAP2K preferences and the specific upstream triggers of some MAP3Ks remain elusive. Thus, to better understand cell fate control by the MAPK network, a systematic single-cell approach capable of monitoring the major MAPK signaling pathways simultaneously and at high temporal resolution is needed. Here, we use live-cell imaging of multiplexed MAPK biosensors to systematically interrogate how the connectivity and dynamics of the MAPK network shape cell fate control in human cells.

RESULTS

To measure MAPK network activity in single cells, we generated a multiplexed reporter system in human breast mammary epithelial cells (MCF10A) that allows for measuring ERK, p38, and JNK activities simultaneously in live cells (Regot et al., 2014) (Figure 1B). Kinase translocation reporters (KTRs) provide highly sensitive measurements of kinase activity through rapid fluorophore translocation and enable real-time signal detection and quantification in thousands of individual cells. Previous work showed that MAPK KTRs are highly specific for their cognate MAPK activity (Regot et al., 2014); therefore, combining ERK, JNK, and p38 biosensors allowed us to measure global MAPK network activity in single cells. Using this new reporter cell line, we recorded MAPK activity dynamics in response to a panel of well-established MAPK activators including osmotic stress (sorbitol, NaCl, and KCI) (Uhlik et al., 2003), oxidative stress (H₂O₂) (Saitoh et al., 1998), ribotoxic stress (anisomycin) (Wu et al., 2020),

Figure 1. Multiplexed reporter system to monitor MAPK activity and dynamics in sinale cells

(A) Schematic of the MAPK core signaling module. MAP3Ks phosphorylate and activate MAP2Ks which in turn activate MAPKs (left). Schematic representing the mammalian MAPK network, where one of the listed MAP3Ks may activate one or more MAP2K which in turn activate MAPKs

(B) Representative images of MCF10A cells expressing H2B-iRFP, ERK-KTR-mCerulean3, JNK-KTR-mRubv2, and p38-KTR-mClover before and after treatment with sorbitol (100 uM) (left). Diagram of "nuclei" and "cytoring" segmentation where each individual cell is marked with another color (right). Scale bars, 20 μm.

growth factors (epidermal growth factor [EGF]), GPCR (G protein-coupled receptor) agonists (S1P) (Spiegel and Milstien, 2003), and cytokines (IL-1 β and TNF- α) (Canovas and Nebreda, 2021; Gantke et al., 2011) (Figures 2A and S1-S3). These stimuli were selected based on

previous MAP3K studies, and concentrations were chosen to maximize MAPK response while minimizing cell death. These seemingly diverse environmental perturbations all elicited activation of more than one MAPK but with quantitatively distinct temporal patterns. Single-cell analysis revealed both digital and analog signaling modes, depending on the stimuli and the MAPK pathway. For example, while EGF, IL-1 β , TNF- α , and S1P mostly elicited short peaks of one or more MAPK activities, anisomycin, hydrogen peroxide, and sorbitol led to longer periods of activity in a dose-dependent manner (Figure S2). Most stimuli triggered the ERK pathway, and this activity was independent of ectodomain shedding by ADAM17, which has been reported to trigger non-cell-autonomous ERK activity (Aikin et al., 2020; Xu and Derynck, 2010) (Figure S3). As most of these MAPK stimuli activated multiple MAPK pathways, we set out to determine whether these stimuli activate multiple MAP3Ks or whether MAP3Ks activate multiple MAPKs.

med intensity nuclei

To address this question, we aimed to block individual MAP3K activities and monitored the resulting MAPK activities upon stimulation. Non-redundant MAP3Ks (COT, TAK, and ZAK) were ablated using CRISPR KOs, and redundant groups of MAP3K activities (MLKs, RAFs, MEKKs, and ASKs) were inhibited using specific small-molecule inhibitors (Figure S3). Results showed that the MAPK response to most stimuli could be extinguished en bloc by eliminating/ablating one MAP3K or MAP3K family (Figure 2B). There were two notable exceptions: (1) EGF-induced MAPK activities were shortened, but not abolished, in the presence of RAF and MLK inhibitors, suggesting that multiple parallel MAP3K activities are engaged upon epidermal growth factor receptor (EGFR) signaling (Figure 2C); and (2) TNF- α and IL-1 β signaling were fully abolished in TAKKO cells but also partially abolished in COTKO cells, suggesting sequential activation of TAK and COT upon cytokine signaling (Figures 2B and 2D). These data are consistent with previous reports (Chadee and

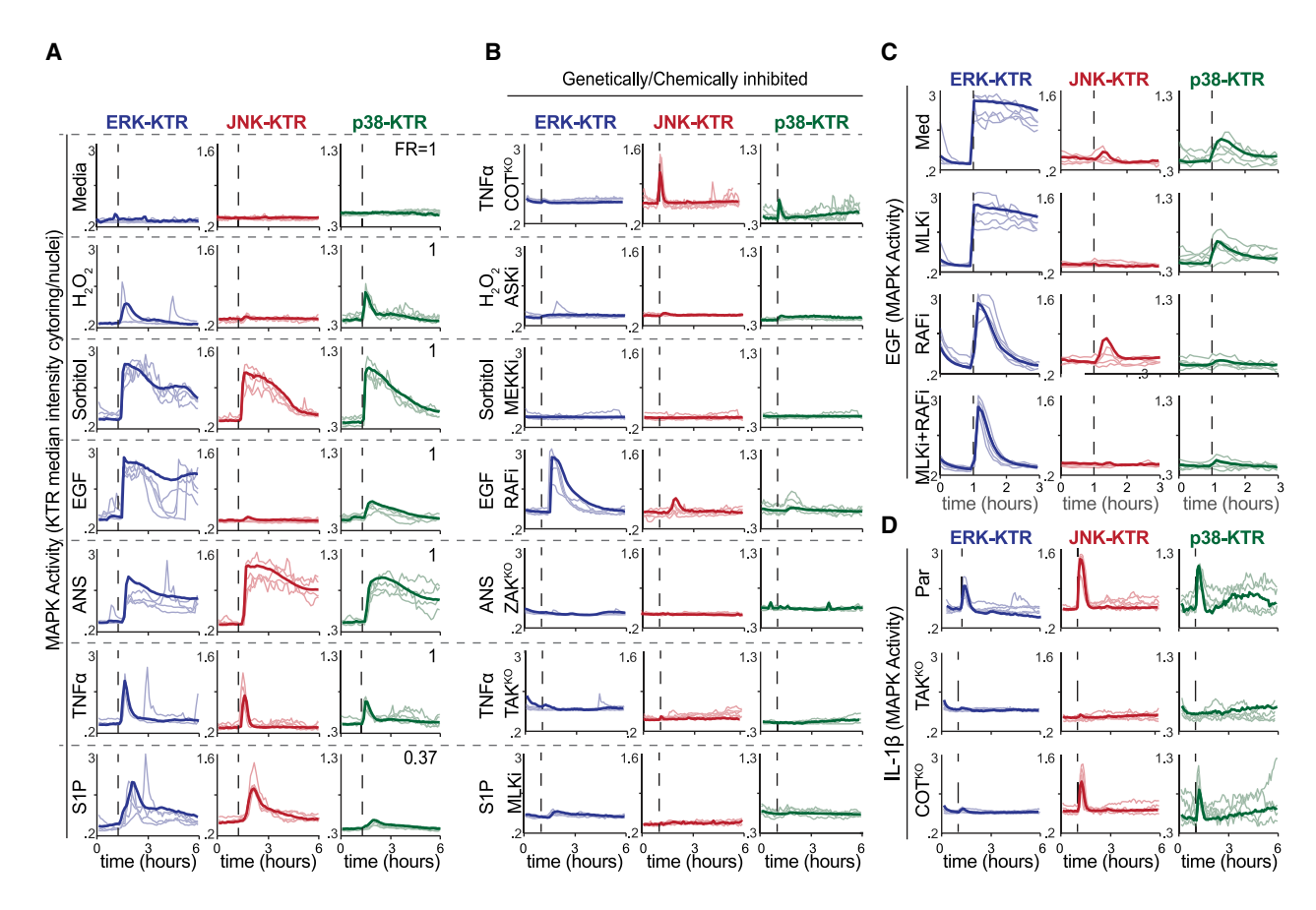


Figure 2. Physiological stimuli activate multiple MAPK pathways through single or multiple MAP3Ks

(A and B) Serum-starved MCF10A MAPK reporter cells were stimulated with media control, (10 ng/mL), hydrogen peroxide (10 μM), sorbitol (100 μM), EGF (10 ng/mL), hydrogen peroxide (10 μM), sorbitol (100 μM), EGF (10 ng/mL), hydrogen peroxide (10 μM), sorbitol (100 μM), EGF (10 ng/mL), hydrogen peroxide (10 μM), sorbitol (100 μM), EGF (10 ng/mL), hydrogen peroxide (10 μM), sorbitol (100 μM), EGF (10 ng/mL), hydrogen peroxide (10 μM), sorbitol (100 μM), EGF (10 ng/mL), hydrogen peroxide (10 μM), sorbitol (100 μM), EGF (10 ng/mL), hydrogen peroxide (10 μM), sorbitol (100 μM), EGF (10 ng/mL), hydrogen peroxide (10 μM), sorbitol (100 μM), EGF (10 ng/mL), hydrogen peroxide (10 μM), sorbitol (100 μM), EGF (10 ng/mL), hydrogen peroxide (10 μM), sorbitol (100 μM), EGF (10 ng/mL), hydrogen peroxide (10 μM), sorbitol (100 μM), EGF (10 ng/mL), hydrogen peroxide (10 μM), sorbitol (100 μM), EGF (10 ng/mL), hydrogen peroxide (10 μM), sorbitol (100 μM), EGF (10 ng/mL), hydrogen peroxide (10 μM), sorbitol (100 μM), EGF (10 ng/mL), hydrogen peroxide (10 μM), sorbitol (100 μM), EGF (10 ng/mL), hydrogen peroxide (10 μM), sorbitol (100 μM), hydrogen peroxide (10 μM), hydrogen peroxide mL), anisomycin (100 ng/mL), TNF- α (10 ng/mL), or sphingosine-1-phosphate (100 μ M), imaged every 5 min for 6 h and quantified as described in STAR Methods. Five representative single-cell traces of the cytoplasmic to nuclear ratio of each KTR are plotted over time and overlaid with the average traces (>350 cells per condition). Fraction of responders (FRs) is indicated. (B) Cells were treated or stimulated with the same inputs as in (A), in the presence of indicated MAP3K inhibitors.

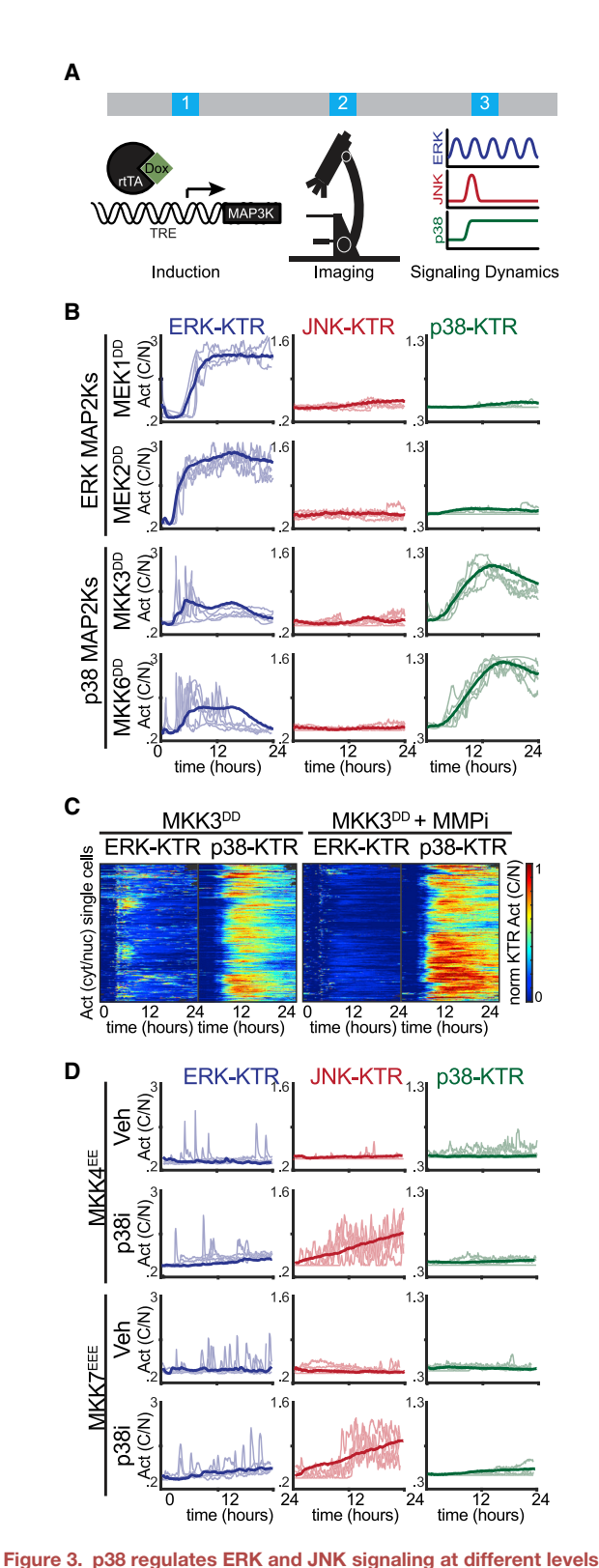
(C) Serum-starved MCF10A cells were treated with EGF (10 ng/mL) in the presence of RAF inhibitor (TAK632) and/or MLK inhibitor (URMC-099) and imaged every 5 min for 3 h. Five representative single-cell traces of KTR activity (cytoplasmic/nuclear ratio) were plotted over time and overlaid with the average traces (n > 800 cells/condition).

(D) Parental, TAKKO, or COTKO serum-starved MCF10A reporter cell lines were treated with IL-1β (10 ng/mL) and imaged every 5 min over 6 h. Plots were quantified as in (A) (n > 500 cells per conditions).

Kyriakis, 2004a, 2004b; Dumitru et al., 2000). Taken together and given the three-tiered topology of MAPK pathways, our results suggest that both the stimuli and the MAP3Ks themselves can activate multiple MAPK pathways simultaneously.

Environmental stresses can damage cells in multiple ways (e.g., UV radiation causes DNA damage, ribotoxic stress, and oxidative stress), thus eliciting different yet simultaneous signaling responses. Thus, to isolate the signaling outputs of different nodes in the MAPK network, we transitioned to a genetic overexpression system. First, we focused on isolating MAP2K activities to interrogate their immediate outputs and feedback regulatory mechanisms. To address this, we generated clonal cell lines containing hyperactive MAP2Ks (i.e., containing phosphomimetic mutations in the activation loop) under the control of a tet-inducible promoter (TRE3G); then we quantified MAPK activity dynamics during MAP2K overexpression via live imaging (Figure 3A). As expected, the cognate MAP2Ks for ERK and p38 (MEK1/2 and MAP2K3/6, respectively) triggered sustained activation of the expected KTR. Notably, p38 activation using MKK3^{DD} expression caused some ERK signaling, especially in cells that activated p38 later in time (Figure 3B). These signaling events were abolished using a matrix metalloprotease (MMP) inhibitor (Batimastat) (Figure 3C), indicating non-cell-autonomous activation of ERK by p38, which concurs with previous studies (Aikin et al., 2020; Xu and Derynck, 2010). In contrast to the ERK and p38 MAP2Ks, the JNK cognate MAP2Ks (MAP2K4 and MAP2K7) did not activate the JNK pathway through overexpression of hyperactive mutants (Figure 3D). Since previous studies have shown p38 inhibition of JNK (Miura et al., 2018), we hypothesized that basal p38 activity could be interfering with full JNK activation from MAP2K4/7. Indeed, both MAP2K4 and MAP2K7 activated the JNK pathway in the presence of a p38 inhibitor (Figure 3D). The resulting JNK activity was highly pulsatile, suggesting additional negative feedback regulation from JNK itself. Overall, this genetic approach revealed cell and non-cell-autonomous activities as well as





(A) Schematic of the systematic overexpression system.
(B and C) Serum-starved MCF10A cells containing indicated TRE3G::MAP2K

(B and C) Serum-starved MCF10A cells containing indicated TRE3G::MAP2K hyperactive constructs were treated with doxycycline (2 μg/mL), imaged for 24 h over 5-min intervals. (B) Five representative single-cell activity traces are overlaid with the average (>350 cells per condition). (C) Heatmaps depicting single-cell traces of ERK- and p38-KTR activity (>350 cells per condition).

prevalent cross talk between MAPK pathways, highlighting the need for an integrated analysis of the network as a whole.

Previous studies showed that overexpression of MAP3Ks activate downstream signaling. This approach has the advantage of isolating the output of individual MAP3Ks while minimizing confounding effects of extracellular stimuli. On the other hand, overexpression can lead to off-target effects by engaging in low-affinity interactions. However, since high-affinity interactions will, by definition, occur at a lower expression level than low-affinity ones, real-time analysis of downstream MAPK activity during expression of the MAP3Ks ensures that the MAP3K output is recorded at the minimal overexpression required. Thus, we generated a collection of 21 stable clonal cell lines, each capable of overexpressing a single MAP3K while reporting ERK, JNK, and p38 activity (Figures S4 and S5). Our cell line collection contains 21 out of 26 MAP3Ks encoded by the human genome and covers all the phylogenetically related groups of MAP3Ks. Overexpression of individual MAP3Ks triggered unique combinations of MAPK activities that were preserved within phylogenetically related kinases (Figures 4A and S6; Video S1): (1) RAFs preferentially activated ERK, (2) ASKs activated p38, (3) ZAK and TAK activated JNK and p38 to a lesser extent, (4) COT activated ERK and p38, (5) mixed lineage kinases (MLKs) activated ERK and JNK, and (6) MEKKs activated all three MAPK branches ERK, JNK, and p38 with simultaneous pulses of activity (Figure S7). Remarkably, we noted qualitative and quantitative similarities between the signaling patterns elicited by natural stimulation (Figures 2A and 2B) and the patterns elicited by MAP3K overexpression (Figure 4A). Once again, these patterns were largely preserved in the absence of ectodomain shedding, although in some cases the ERK activity was diminished or abolished indicating non-cell-autonomous ERK activity (Figure S8). Phosphorylation patterns of MEK1/2, MKK3/6, and MKK7 were in agreement with cognate MAPK activation (Figure S9). Of note, COT or ASK induction showed MKK4 phosphorylation (Figure S9) but not JNK activity, as reported by the JNK KTR (Figure 4A). However, p38 inhibition during expression of these MAP3Ks triggered pulses of JNK activity similar to the ones observed upon MKK4/7 overexpression (Figures 3C and 4C). This result suggests that JNK activity can be masked by p38 in response to MKK4 activation. By contrast, all the MAP3Ks that activate JNK in addition to p38 also show MKK7 phosphorylation, suggesting that the JNK phosphorylation by MKK4 is more sensitive to p38 regulation than MKK7-dependent JNK activation. Overall, we also noted a difference between the two phylogenetically distinct groups of MAP3Ks, the STE and the TKL MAP3Ks (Figure 4E). While STEs preferentially activate p38 and ERK combinations, TKLs preferentially activate JNK and ERK combinations (Figures 4B and 4D). The vast differences in signaling preferences between the STE and TKL kinases reflect their early (eukaryotic) divergence within the human kinome tree (Figure 4E).

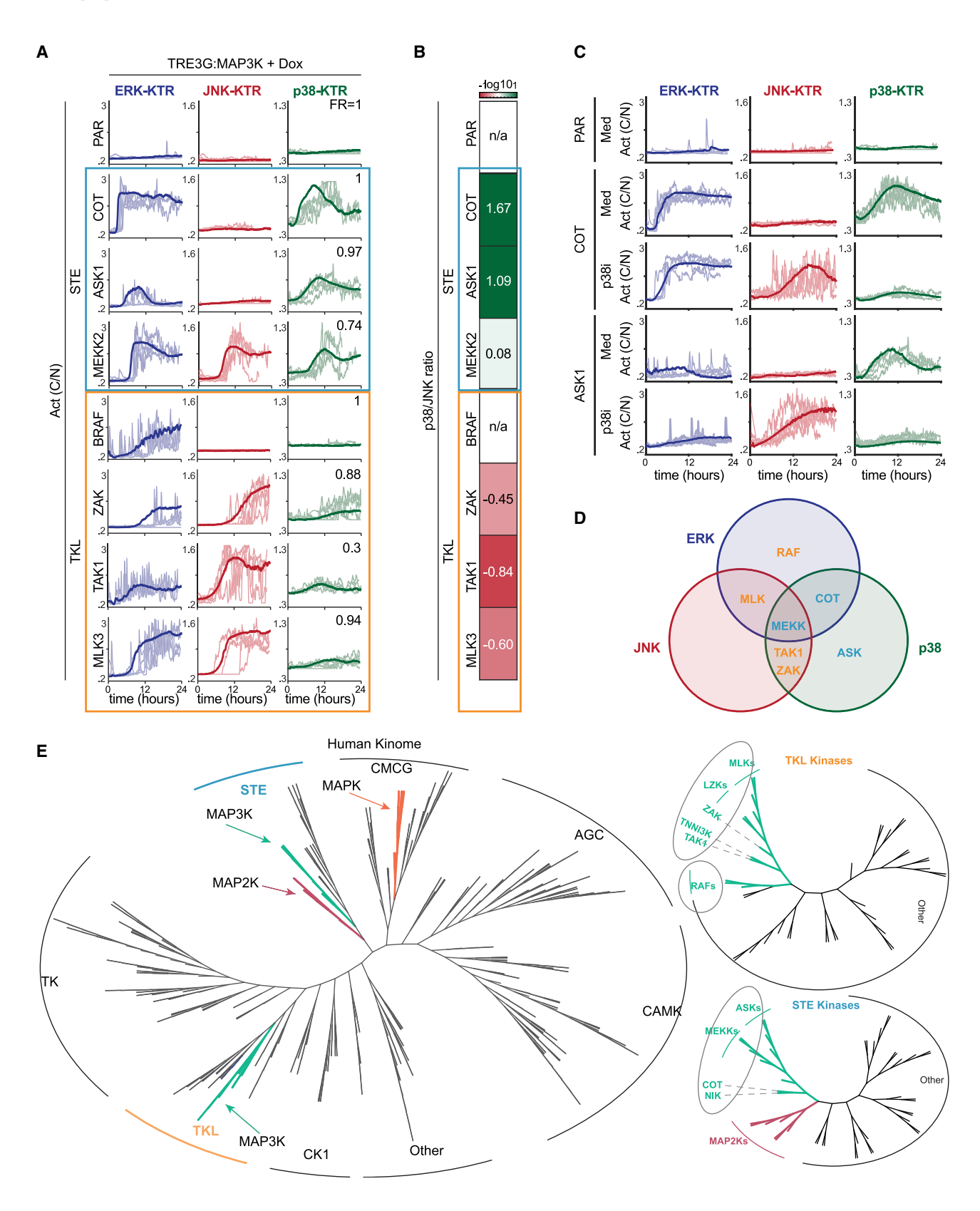
Next, we wanted to understand the physiological role of the different MAPK activity combinations observed. Global gene

(D) Serum-starved MCF10A cells containing indicated that TRE3G::MAP2K hyperactive constructs were treated with doxycycline (2 μ g/mL), imaged for 24 h over 5-min intervals. Five representative single-cell activity traces are overlaid with the average (>400 cells per condition).

Cell Systems Article







(legend on next page)



expression analysis indeed showed different gene expression programs that separate according to MAPK activity patterns (Figures 5A and S10). In addition to transcriptomics, we measured cell fates that are regulated by MAPK signaling, including cell proliferation, migration, and apoptosis. An exhaustive analysis of cell proliferation measured by endpoint 5-ethynyl-2 deoxyuridine (EdU) incorporation, phosphor-Rb, Myc, and p21 immunofluorescence showed that whereas the ERK + p38 combination blocks proliferation, the ERK + JNK combination increased proliferation by 10-fold, about an order of magnitude more than with ERK activity alone (Figure 5B). Similar combinatorial effects were observed when measuring apoptosis with live measurements of caspase-3/7; whereas the ERK + p38 combination inhibited apoptosis, the JNK + p38 combination increased apoptosis (Figure 5C). Since each MAPK combination was triggered by induction of a different MAP3K, one possibility is that other downstream effects of these MAP3Ks are responsible for the observed cell fate differences. To address this possibility, we hypothesized that using the triple MAPK activators (MEKKs) (Figure 4A) in the presence of specific MAPK inhibitors would allow us to direct cells into different fates in a predictable manner. Indeed, artificial induction of the ERK + JNK activity pattern, using the triple MAPK activator MEKK2 in the presence of p38 inhibitor, phenocopied the MLK cell-cycle increase (Figure 5D). Both ERK and JNK activities were necessary for the observed cell-cycle increase (Figure 5D). Similarly, using both MLK and MEKK inductions in the presence of ERK inhibitor induced massive JNK-dependent apoptosis (Figure 5E). Taken together, this analysis suggests that MAP3K-driven combinations of MAPK activities control cell fate.

To further explore this idea in a more physiological context, we examined how MAPK combinations influence proliferation and programmed cell death in response to environmental perturbations. In particular, we focused on MLK signaling that preferentially activates the ERK + JNK activity combination (Figure 4A) and promotes proliferation of MCF10A cells (Figure 5B). Thus, to directly visualize cell-cycle entry while quantifying MLK signaling, we generated a new reporter cell line expressing the ERK and JNK biosensors together with a CDK2 activity biosensor that allows measuring the proliferation quiescence decision in single cells (Spencer et al., 2013). Results showed that cells that exit quiescence in response to EGF or S1P stimulation have significantly higher MLK-driven JNK signaling (Figures 6A and 6B). Of note, blocking either ERK or JNK with specific inhibitors was sufficient to abolish the proliferative effects of these stimuli (Figures 6C and 6D). This data suggest that the MLKdriven ERK + JNK combination promotes exit from quiescence in epithelial cells. To test this hypothesis during natural stimulation, we used osmotic stress, which normally activates all three MAPK pathways, in the presence or absence of a p38 inhibitor. Results showed that indeed p38 inhibition upon osmostress leads to increased proliferation (Figure S11). Finally, we argued that if the difference between pro-proliferation and pro-apoptotic signaling depends on the presence of ERK activity, inhibition of ERK upon S1P signaling would redirect cell fate from proliferation to apoptosis. Indeed, S1P stimulation in the presence of ERK inhibitor caused widespread apoptosis (Figure 6E). Similarly, TNF- α stimulation in WT or COTKO cells showed that eliminating the ERK signal in the COTKO results in elevated apoptosis (Figure 6E). Overall, our data indicate that JNK-mediated cell fate decisions depend on the global MAPK signaling state of the cell (Figures 6F and S12). When ERK signaling is inactive, JNK promotes apoptosis; however, in the presence of ERK activity, cells are protected from apoptosis and JNK activity enables cell-cycle entry. Together with the finding that MAP3Ks elicit unique combinations of MAPK activities, we propose that MAP3Ks drive cell fate choices by combinatorial control of MAPK activity.

DISCUSSION

Through systematic genetic and chemical perturbations paired with live imaging, we determined that extracellular stimuli elicit distinct configurations of downstream ERK, JNK, and p38 MAPK activity and that these combinations are largely dependent on the MAP3K mediating the signal. We combined an artificial overexpression system with the use of natural stimuli and found that, in both cases, the activation of MAPKs in isolation is rare and that the combined activity of ERK + JNK has different functional outcomes than ERK or JNK alone. These findings suggest that combinatorial MAPK signaling downstream of a specific MAP3K leads to changes in cell behavior. Thus, our studies place MAP3Ks as critical nodes of input-output specificity within the MAPK network. Even though MAPKs have been extensively studied, the MAP3Ks that mediate signaling are often less understood. In fact, we know very little about the upstream activators of most MAP3Ks (with the exception of RAFs, ASKs, and ZAKs). We propose that identifying the MAP3Ks that mediate signaling in different contexts will enable a better understanding of the input-output specificity of this clinically relevant network. As an example, recent studies to understand the ribotoxic stress response through the MAP3K ZAK have identified a critical role for ribosome collisions in controlling cell fate upon environmental stress (Wu et al., 2020). Future studies centered on other MAP3Ks and their primary upstream triggers are needed to understand the underlying logic of the MAPK signaling network.

Figure 4. MAP3Ks elicit unique combinations of MAPK activity

(A) Serum-starved MCF10A cells containing indicated that TRE3G::MAP3K constructs were treated with doxycycline (2 μg/mL), imaged for 24 h over 5-min intervals, and quantified as the ratio cytoplasmic over nuclear KTR intensity. Five representative single-cell activity traces are overlaid with the average (>350 cells per condition).

⁽B) Ratio of p38 to JNK was calculated by dividing P38/JNK biosensor activity. Heatmap illustrating the P38/JNK activity ratios in each MAP3K induction.

⁽C) Serum-starved MCF10A cells containing ASK1 or COT were treated with doxycycline (2 µg/mL) in the presence or absence of p38 inhibitor (SB203580) and imaged every 5 min for 24 h. Four representative single-cell traces of the cytoplasmic to nuclear ratio of each KTR are plotted over time.

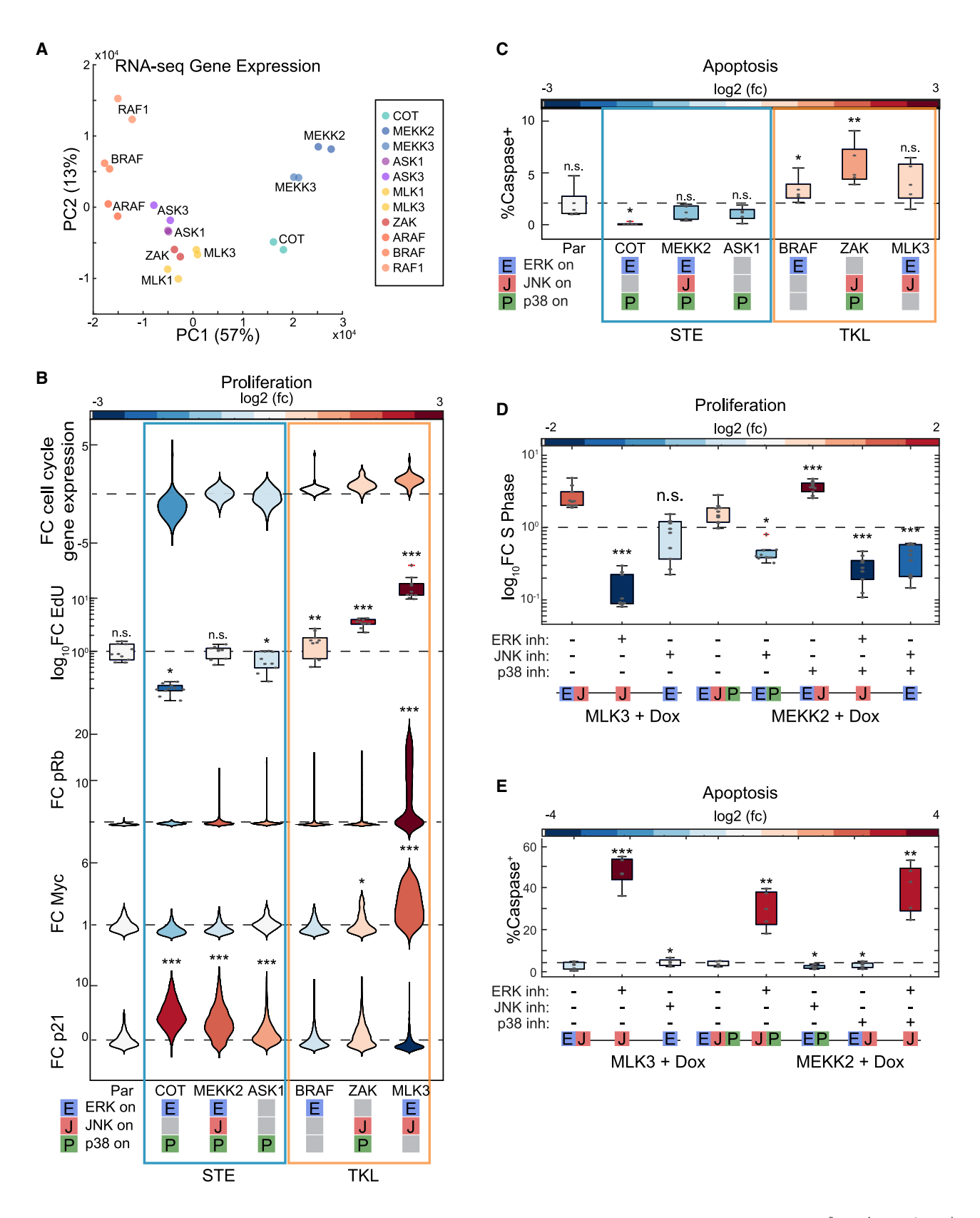
⁽D) Venn diagram representing the signaling activities of each MAP3K.

⁽E) Adapted from the human kinome tree. Unrooted phylogenetic relationship of all human protein kinases. Green lines indicate MAP3Ks, pink indicates MAP2Ks, and orange indicates MAPKs. Right: unrooted trees representing the phylogenetic relationships of the STE kinases (top) and TKL kinases (bottom), adapted from the human kinome tree (Cell Signaling Technology [CST]).

Cell Systems Article







(legend on next page)



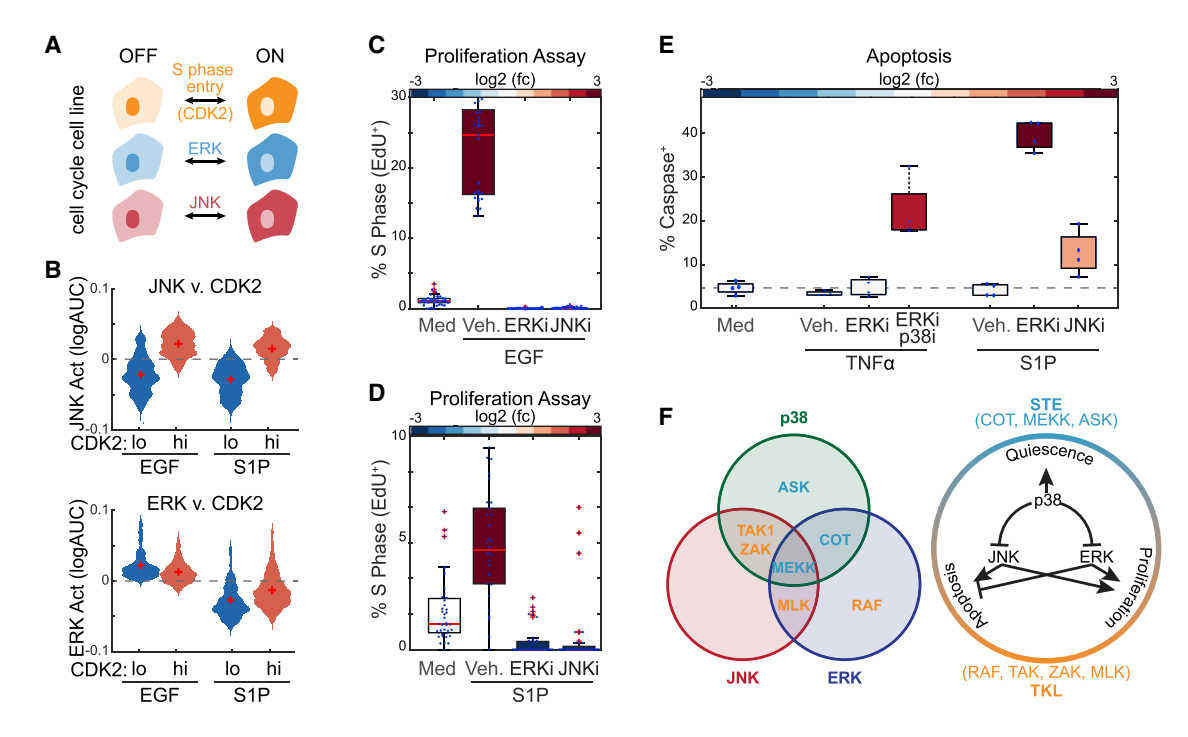


Figure 6. TKL kinases coordinate single-cell fates in multicellular contexts

(A) Schematic of multiplexed cell line containing reporters for CDK2, ERK, or JNK activity.

(B) Serum-starved MCF10A cells were stimulated with EGF or S1P and imaged every 5 min for 24 h. Distribution plots indicate the average JNK or ERK activity in cells that have low or high CDK2 activity (n > 600 cells).

(C and D) Serum-starved cells were treated with indicated inhibitors or vehicle control. Cells were treated with EGF (10 ng/mL) (C) or sphingosine-1-phosphate (100 µM) (D). After 20 h, cells were incubated with EdU for 4 h before fixation. Boxplots represent relative percentage of cells in the S phase, as normalized to the vehicle control.

(E) Serum-starved cells were incubated with caspase dye as described in Figure 1 and treated with JNK inhibitor or vehicle control. Cells were then treated with TNF- α (10 ng/mL) or sphingosine-1-phosphate (100 μ M). Relative apoptotic rates are quantified as described in STAR Methods.

(F) Schematic depicting MAP3K specificities toward ERK, JNK, or p38 (left) and the cell fates associated with each combination of MAPK activation (right). P values were quantified using two-way ANOVA (C–E). *p < 0.05, **p < 0.01, and ***p < 0.001.

We found that many inputs and MAP3Ks exhibit promiscuity within the MAPK network. We find that all MAP3Ks activate the ERK pathway through either cell-autonomous or non-cell-autonomous mechanisms. This widespread ERK activation is likely to contribute to cancer progression beyond the RAS-RAF-driven tumorigenesis. Indeed, many different MAP3Ks (COT, MLK, TAK1, ZAK, and MEKK) have been shown to contribute to drug resistance to RAF inhibition (Cuevas et al., 2006; Johannessen et al., 2010; Li et al., 2018; Marusiak et al., 2014). These studies

further highlight the importance of understanding MAP3Ks in disease progression.

Many human diseases, from cancer to autoimmunity, are disorders of dysregulated multicellularity. The two phylogenetically distinct groups of MAP3Ks, the sterile (STE) and tyrosine kinaselike (TKL) MAP3Ks, which are related by sequence homology to the yeast MAP3Ks or tyrosine kinases, respectively, also appear to be differentially activated by environmental stress (oxidative stress, ASK; osmotic stress, MEKKs) or cytokines/growth factors

Figure 5. MAP3Ks coordinate cell fate through combinations of MAPK activity

(A) PCA of RNA sequencing results of indicated MAP3K inductions.

(B) Cell fate analysis by RNA sequencing (fold-change cell-cycle markers), EdU incorporation, and immunofluorescence (pRb, Myc, and p21), as described in STAR Methods. Violin or boxplots represent the relative changes in cell fate, colors represent the log₂ fold change over the parental (see STAR Methods for details) (n > 2,000 cells for all imaging assays).

(C) Cell fate analysis by RNA sequencing, live imaging (deltaX-Y [dXY], caspase dye) violin or boxplots represent the relative changes in cell fate, colors represent the log₂ fold change over the parental (see STAR Methods for details) (n > 250 cells per live conditions).

(D) MCF10A cells containing TRE3G::MLK3 or TRE3G::MEKK2 were grown to confluence before overnight serum starvation and treatment with doxycycline (2 µg/mL) and indicated inhibitor or vehicle control. Boxplots represent fold change of EdU+ cells in each condition over the no doxycycline control. Statistical significance was determined over the doxycycline + vehicle of a given cell line.

(E) Serum-starved MCF10A cells containing TRE3G::MLK3 or TRE3G::MEKK2 were treated with vehicle control or indicated inhibitor combination and doxycycline (2 μ g/mL) and imaged every 5 min for 24 h in media containing 10 μ M CellEvent Caspase-3/7 Green Detection Reagent (see STAR Methods for details). Boxplots indicating the percentage of cells in each technical replicate that initiate apoptosis. Colors indicate the fold change over the no doxycycline control for that cell line (n > 800 cells per condition). For all boxplots, p values were quantified using two-way ANOVA. For all violin plots, p values were quantified using two-way ANOVA and a Bonferroni correction. *p < 0.05, **p < 0.01, and ***p < 0.001.



(cytokines, TAK; growth factors, RAF, MLKs) (Figure 2). In addition, we found that STE and TKL MAP3Ks preferentially activate the SAPKs, p38, and JNK, respectively (Figure 4). With regard to cell fate, the STE MAP3Ks drive cell-cycle arrest and survival, thereby promoting unicellular fitness. However, the TKL MAP3Ks promote cell-cycle progression or apoptosis. Taken together, it is tempting to speculate that the evolution of the MAPK signaling network played an important role in the unicellular to multicellular transition. In fact, recent efforts in defining the evolutionary transitions that enabled multicellularity suggest that rewiring of signaling networks may have played a critical role (Sebé-Pedrós et al., 2017; Suga et al., 2014).

Overall, this study represents an unprecedented analysis of MAPK signaling network dynamics. Our findings reveal an essential role for MAP3Ks in driving cell fate through combinations of MAPK activity. We anticipate that future network-level studies considering different signaling hubs simultaneously will enable a better understanding of the fundamentals of signaling-mediated control of cell fate.

STAR*METHODS

Detailed methods are provided in the online version of this paper and include the following:

- KEY RESOURCES TABLE
- RESOURCE AVAILABILITY
 - Lead contact
 - Materials availability
 - Data and code availability
- EXPERIMENTAL MODEL AND SUBJECT DETAILS
 - Cell Lines
- METHOD DETAILS
 - Live Imaging
 - Image Analysis and Quantification
 - Immunoblotting
 - Cell Death Assay
 - Experimental replicates and statistical power

SUPPLEMENTAL INFORMATION

Supplemental information can be found online at https://doi.org/10.1016/j. cels.2022.10.003.

ACKNOWLEDGMENTS

We thank all members of the Regot lab for technical and theoretical support throughout the project, and for commentary and edits on the final manuscript. We would especially like to thank our lab manager, Lea Fortuno-Miranda, for her technical support. We acknowledge our funding sources: NIH NIGMS R35(1R35GM133499), NSF CAREER award (MCB-1844994), American Cancer Society Research Scholar Grant (133537-RSG-19-005-01-CCG), and Jerome L. Greene Foundation Discovery Award to S.R.

AUTHOR CONTRIBUTIONS

S.R. and A.F.P. conceived the project. A.F.P. and K.I. performed MCF10A experiments. A.F.P. performed image analysis. S.R. and A.F.P. wrote and edited the final manuscript. E.J.H., J.P., C.M., and G.S.B. provided support, commentary, and edits. S.R. supervised the project and secured funding.

DECLARATION OF INTERESTS

The authors declare no competing interests.

Received: April 21, 2022 Revised: August 15, 2022 Accepted: October 17, 2022 Published: November 9, 2022

REFERENCES

Aikin, T.J., Peterson, A.F., Pokrass, M.J., Clark, H.R., and Regot, S. (2020). MAPK activity dynamics regulate non-cell autonomous effects of oncogene expression. eLife 9, e60541.

Arthur, J.S., and Ley, S.C. (2013). Mitogen-activated protein kinases in innate immunity. Nat. Rev. Immunol. 13, 679-692.

Campeau, E., Ruhl, V.E., Rodier, F., Smith, C.L., Rahmberg, B.L., Fuss, J.O., Campisi, J., Yaswen, P., Cooper, P.K., and Kaufman, P.D. (2009). A versatile viral system for expression and depletion of proteins in mammalian cells. PLoS One 4, e6529.

Canovas, B., and Nebreda, A.R. (2021). Diversity and versatility of p38 kinase signalling in health and disease. Nat. Rev. Mol. Cell Biol. 22, 346-366.

Chadee, D.N., and Kyriakis, J.M. (2004a). MLK3 is required for mitogen activation of B-Raf, ERK and cell proliferation. Nat. Cell Biol. 6, 770-776.

Chadee, D.N., and Kyriakis, J.M. (2004b). A novel role for mixed lineage kinase 3 (MLK3) in B-Raf activation and cell proliferation. Cell Cycle 3, 1227-1229.

Cuevas, B.D., Winter-Vann, A.M., Johnson, N.L., and Johnson, G.L. (2006). MEKK1 controls matrix degradation and tumor cell dissemination during metastasis of polyoma middle-T driven mammary cancer. Oncogene 25, 4998-5010.

Dhillon, A.S., Hagan, S., Rath, O., and Kolch, W. (2007). MAP kinase signalling pathways in cancer. Oncogene 26, 3279-3290.

Dumitru, C.D., Ceci, J.D., Tsatsanis, C., Kontoyiannis, D., Stamatakis, K., Lin, J.H., Patriotis, C., Jenkins, N.A., Copeland, N.G., Kollias, G., and Tsichlis, P.N. (2000). TNF-alpha induction by LPS is regulated posttranscriptionally via a Tpl2/ERK-dependent pathway. Cell 103, 1071-1083.

Fey, D., Croucher, D.R., Kolch, W., and Kholodenko, B.N. (2012). Crosstalk and signaling switches in mitogen-activated protein kinase cascades. Front. Physiol. 3, 355.

Galcheva-Gargova, Z., Dérijard, B., Wu, I.H., and Davis, R.J. (1994). An osmosensing signal transduction pathway in mammalian cells. Science 265, 806-808.

Gantke, T., Sriskantharajah, S., and Ley, S.C. (2011). Regulation and function of TPL-2, an IkB kinase-regulated MAP kinase kinase kinase. Cell Res. 21, 131-145.

Gibson, D.G., Young, L., Chuang, R.Y., Venter, J.C., Hutchison, C.A., 3rd, and Smith, H.O. (2009). Enzymatic assembly of DNA molecules up to several hundred kilobases. Nat. Methods 6, 343-345.

Han, J., Lee, J.D., Bibbs, L., and Ulevitch, R.J. (1994). A MAP kinase targeted by endotoxin and hyperosmolarity in mammalian cells. Science 265, 808–811.

Heinrichsdorff, J., Luedde, T., Perdiguero, E., Nebreda, A.R., and Pasparakis, M. (2008). p38 alpha MAPK inhibits JNK activation and collaborates with IkappaB kinase 2 to prevent endotoxin-induced liver failure. EMBO Rep. 9,

Johannessen, C.M., Boehm, J.S., Kim, S.Y., Thomas, S.R., Wardwell, L., Johnson, L.A., Emery, C.M., Stransky, N., Cogdill, A.P., Barretina, J., et al. (2010). COT drives resistance to RAF inhibition through MAP kinase pathway reactivation. Nature 468, 968-972.

Johnson, G.L., and Lapadat, R. (2002). Mitogen-activated protein kinase pathways mediated by ERK, JNK, and p38 protein kinases. Science 298,

Kyriakis, J.M., and Avruch, J. (2012). Mammalian MAPK signal transduction pathways activated by stress and inflammation: a 10-year update. Physiol. Rev. 92, 689-737.





La Marca, J.E., and Richardson, H.E. (2020). Two-faced: roles of JNK signalling During tumourigenesis in the drosophila model. Front. Cell Dev. Biol. 8, 42. Li, L., Su, N., Zhou, T., Zheng, D., Wang, Z., Chen, H., Yuan, S., and Li, W. (2018). Mixed lineage kinase ZAK promotes epithelial-mesenchymal transition in cancer progression. Cell Death Dis. 9, 143.

Manning, G., Whyte, D.B., Martinez, R., Hunter, T., and Sudarsanam, S. (2002). The protein kinase complement of the human genome. Science 298, 1912-1934.

Marusiak, A.A., Edwards, Z.C., Hugo, W., Trotter, E.W., Girotti, M.R., Stephenson, N.L., Kong, X., Gartside, M.G., Fawdar, S., Hudson, A., et al. (2014). Mixed lineage kinases activate MEK independently of RAF to mediate resistance to RAF inhibitors. Nat. Commun. 5, 3901.

McCubrey, J.A., Steelman, L.S., Chappell, W.H., Abrams, S.L., Wong, E.W., Chang, F., Lehmann, B., Terrian, D.M., Milella, M., Tafuri, A., et al. (2007). Roles of the Raf/MEK/ERK pathway in cell growth, malignant transformation and drug resistance. Biochim. Biophys. Acta 1773, 1263-1284.

Miura, H., Kondo, Y., Matsuda, M., and Aoki, K. (2018). Cell-to-cell heterogeneity in p38-mediated cross-inhibition of JNK causes stochastic cell death. Cell Rep. 24, 2658-2668.

Regot, S., Hughey, J.J., Bajar, B.T., Carrasco, S., and Covert, M.W. (2014). High-sensitivity measurements of multiple kinase activities in live single cells. Cell 157, 1724-1734.

Saitoh, M., Nishitoh, H., Fujii, M., Takeda, K., Tobiume, K., Sawada, Y., Kawabata, M., Miyazono, K., and Ichijo, H. (1998). Mammalian thioredoxin is a direct inhibitor of apoptosis signal-regulating kinase (ASK) 1. EMBO J. 17, 2596-2606.

Sebé-Pedrós, A., Degnan, B.M., and Ruiz-Trillo, I. (2017). The origin of Metazoa: a unicellular perspective. Nat. Rev. Genet. 18, 498-512.

Spencer, S.L., Cappell, S.D., Tsai, F.C., Overton, K.W., Wang, C.L., and Meyer, T. (2013). The proliferation-quiescence decision is controlled by a bifurcation in CDK2 activity at mitotic exit. Cell 155, 369-383.

Spiegel, S., and Milstien, S. (2003). Sphingosine-1-phosphate: an enigmatic signalling lipid. Nat. Rev. Mol. Cell Biol. 4, 397-407.

Suga, H., Torruella, G., Burger, G., Brown, M.W., and Ruiz-Trillo, I. (2014). Earliest Holozoan expansion of phosphotyrosine signaling. Mol. Biol. Evol. 31, 517-528.

Tournier, C. (2013). The 2 faces of JNK signaling in cancer. Genes Cancer 4, 397-400.

Uhlik, M.T., Abell, A.N., Johnson, N.L., Sun, W., Cuevas, B.D., Lobel-Rice, K.E., Horne, E.A., Dell'Acqua, M.L., and Johnson, G.L. (2003). Rac-MEKK3-MKK3 scaffolding for p38 MAPK activation during hyperosmotic shock. Nat. Cell Biol. 5, 1104–1110.

Ventura, J.J., Hübner, A., Zhang, C., Flavell, R.A., Shokat, K.M., and Davis, R.J. (2006). Chemical genetic analysis of the time course of signal transduction by JNK. Mol. Cell 21, 701-710.

Wagner, E.F., and Nebreda, A.R. (2009). Signal integration by JNK and p38 MAPK pathways in cancer development. Nat. Rev. Cancer 9, 537-549.

Wu, C.C., Peterson, A., Zinshteyn, B., Regot, S., and Green, R. (2020). Ribosome collisions trigger General Stress responses to regulate cell fate. Cell 182, 404-416.e14.

Xu, P., and Derynck, R. (2010). Direct activation of TACE-mediated ectodomain shedding by p38 MAP kinase regulates EGF receptor-dependent cell proliferation. Mol. Cell 37, 551-566.

Cell Systems Article



STAR***METHODS**

KEY RESOURCES TABLE

REAGENT or RESOURCE	SOURCE	IDENTIFIER
Antibodies		
Mouse monoclonal anti-MEK1/2	Cell Signaling Technology	Cat#4694 (L38C12); RRID:AB_10695868
Rabbit monoclonal anti-Phospho-MEK1/2 (Ser217/221)	Cell Signaling Technology	Cat#9154 (41G9); RRID:AB_2138017
MEK7 (phospho S271 + T275) antibody	Abcam	Cat#4762; RRID:AB_304598
Rabbit monoclonal anti-Phospho-SEK1/ MKK4 (Ser257)	Cell Signaling Technology	Cat#4514S (C36C11); RRID:AB_2140946
Mouse monoclonal anti-HSC 70	Santa Cruz Biotechnology	Cat#7298; RRID:AB_627761
IRDye 800CW Donkey anti-Rabbit IgG	Licor	Cat#926-32213; RRID:AB_621848
IRDye 680RD Goat anti-Mouse IgG	Licor	Cat#926-68070; RRID:AB_10956588
Rabbit monoclonal anti-Phospho-MKK3 (Ser189) /MKK6 (Ser207)	Cell Signaling Technology	Cat#9231; RRID:AB_2140799
Rabbit polyclonal anti-COT	Genetex	Cat#GTX102711 [N3C3]; RRID:AB_1950870
Rabbit monoclonal anti-TAK1	Cell Signaling Technology	Cat#5206 (D94D7); RRID:AB_10694079
Chemicals, peptides, and recombinant proteins		
Ulixertinib	Selleck Chemicals	Cat#S7854
Selonsertinib	Selleck Chemicals	Cat#S8292
JRMC-099	Selleck Chemicals	Cat#S7343
ΓΑK-632	Selleck Chemicals	Cat#S7291
Ponatinib	Selleck Chemicals	Cat#S1490
Gefitinib	Selleck Chemicals	Cat#S1025
BIRB-796	Selleck Chemicals	Cat#S1574
JNK-XVI (JNK-inh-8)	MedChem Express	Cat#HY-13319
Cot-inhibitor-1	MedChem Express	Cat#HY-32015
SB-203580	Sigma-Aldrich	Cat#S8307
5Z-7-Oxozeaenol	Sigma-Aldrich	Cat#O9890
Batimastat	Selleck Chemicals	Cat#S7155
ΓΝΕ-α	Gibco	Cat#PHC 3015
L1β	R&D Systems	Cat#201-LB-005
H_2O_2	Thermo Fisher	Cat#H325-500
Sorbitol	Thermo Fisher	Cat#50-70-4
Sodium Chloride	Fisher Scientific	Cat#7647-15-5
KCI	Fisher Scientific	Cat#7447-40-7
Sphingosine-1-phosphate	Fisher Scientific	Cat#13-701
Prostaglandin E2	Millipore Sigma	Cat#P5640
Oleoyl-L-α-lysophosphatidic acid sodium salt	Millipore Sigma	Cat#L7260
Poly(I:C)	Sigma-Aldrich	Cat#P1530
Cyclohexamide	Sigma-Aldrich	Cat#C4859
EGF	PreproTech	Cat#AF-100-15
Anisomycin	Apexbio	Cat#B6674
EdU	Thermo Fisher	Cat#A10044
Critical commercial assays		
RNeasy Micro Kit	Qiagen	Cat#74004
CellEvent Caspase 3/7 Green Dye	Invitrogen	Cat#C1-423

(Continued on next page)





Continued				
REAGENT or RESOURCE	SOURCE	IDENTIFIER		
Deposited data				
Raw and processed RNA sequencing data	This paper	NCBI GEO: GSE213882		
Human reference genome NCBI build 38, GRCh38	Genome Reference Consortium	http://www.ncbi.nlm.nih.gov/projects/ genome/assembly/grc/human/		
Single cell imaging data	This paper	https://github.com/regotlab/MAP3K-signaling/tree/master https://doi.org/10.5281/zenodo.7153234		
Experimental models: Cell lines				
Human MCF 10A	ATCC	Cat#CRL-10317		
Human HEK293FT	Thermo Fisher	Cat#R70007		
Oligonucleotides				
See Table S1		N/A		
Recombinant DNA				
pTA30 PGK:ERK-KTR-mCerulean3 (Hygromycin)	Aikin et al., 2020	N/A		
pSR1846 PGK:JNK-KTR-mRuby2 (Blasticidin)	Regot et al., 2014	N/A		
pAP50 PGK:p38-KTR-mClover	Aikin et al., 2020	N/A		
pSR1881 H2B-iRFP	Regot et al., 2014	N/A		
pAP53 TRE3G:MEK1DD (puro)	Aikin et al., 2020	N/A		
oHC141 TRE3G:MEK2DD (puro)	Aikin et al., 2020	N/A		
oYL49 TRE3G:MAP2K7EEEdeltaN (puro)	This paper	N/A		
bYL47 TRE3G:MAP2K4EEdeltaN (puro)	This paper	N/A		
oAP54 TRE3G:MAP2K5DD (puro)	This paper	N/A		
oAP55 TRE3G:MAP2K3DD (puro)	Aikin et al., 2020	N/A		
oAP128 TRE3G:MAP3K8 (puro)	This paper	N/A		
oAP107 TRE3G:ASK1 (puro)	This paper	N/A		
oAP131 TRE3G:TAK1 (puro)	This paper	N/A		
pAP124 TRE3G:YSK4 (puro)	This paper	N/A		
oAP122 TRE3G:MAP3K15 (puro)	This paper	N/A		
pAP148: TRE3G:TNNI3K (puro)	This paper	N/A		
oAP116: TRE3G:ILK (puro)	This paper	N/A		
pAP95: TRE3G:MEKK2 (puro)	This paper	N/A		
pAP115: TRE3G:ARAF (puro)	This paper	N/A		
pAP111: TRE3G:MAP3K14 (puro)	This paper	N/A		
pAP112: TRE3G:TAOK3 (puro)	This paper	N/A		
oAP114: TRE3G:MAP3K12 (puro)	This paper	N/A		
pAP109: TRE3G:MAP3K13 (puro)	This paper	N/A		
pAP113: TRE3G:MAP3K11 (puro)	This paper	N/A		
pAP93: TRE3G:MAP3K5 kinase domain (puro)	This paper	N/A		
pAP96:TRE3G:MEKK2 kinase domain (puro)	This paper	N/A		
DHB-mVenus	Spencer et al., 2013	Addgene Cat#136461		
pTA70 ADAM17 CRISPR KO Assembly 1 (Neomycin)	Aikin et al., 2020	N/A		
oAP177 MAP3K8 CRISPR KO Assembly 1 (Neomycin)	This paper	N/A		
pAP194 MAP3K7 CRISPR KO Assembly 2 (Neomycin)	This paper	N/A		

(Continued on next page)





Continued		
REAGENT or RESOURCE	SOURCE	IDENTIFIER
Software and algorithms		
MATLAB	MathWorks	www.mathworks.com
Metamorph	Molecular Devices	https://www.metamorphsoftware.com/
Python	Python Software Foundation	www.python.org
Neural Net Segmentation	This paper	https://doi.org/10.5281/zenodo.7153234
CellProfiler	Broad Institute	Cellprofiler.org

RESOURCE AVAILABILITY

Lead contact

Further information and requests for resources and reagents should be directed to and will be fulfilled by the lead contact, Sergi Regot (sregot@jhmi.edu).

Materials availability

All materials will be made available upon request.

Data and code availability

RNA sequencing data sets has been deposited to the NCBI GEO database (GSE213882). Live imaging data of MAP3K inductions and MAPK inputs is available from: https://github.com/regotlab/MAP3K-signaling/tree/master, DOIs are listed in the key resources table. All original code has been deposited at Github and is publically available. DOIs are listed in the key resources table. Any additional information to reanalyze the data reported in this paper is available from the lead contact upon request.

EXPERIMENTAL MODEL AND SUBJECT DETAILS

Cell Lines

MCF10A human mammary epithelial cells (ATCC) were grown at 37° and 5% CO2 in DMEM/F12 (Gibco) with 5% horse serum (HS) (Sigma), 10 µg/ml Insulin (Sigma), 20 ng/ml EGF (Peprotech), 1x Penicillin-Streptomycin (P/S) (Gibco), 0.5 mg/ml Hydrocortisone (Sigma), 100 ng/ml Cholera Toxin (Sigma). Cells were passaged every 3 days with 0.25% Trypsin-EDTA (Gibco), were mycoplasma free, and were verified by STAR-profiling (ATCC).

HEK293-FT cells were cultured in DMEM (Gibco) with 10% fetal bovine serum (FBS; Omega Scientific), 1% MEM non-essential amino acids (NEAA; Gibco), 1% Glutamax (Gibco), 1% MEM sodium pyruvate (Gibco), 1x Penicillin-Streptomycin (P/S) (Sigma), and 500 $\mu g/ml$ Geneticin (Gibco).

METHOD DETAILS

Stable cell lines were generated with lentivirus produced in HEK293-FTs (Thermo) with third-generation packaging plasmids and Lipofectamine 2000 (Thermo). Viral supernatants were collected 48 hours after transfection and incubated in MCF10As with polybrene (10 μg/ml, EMD Millipore). To create multiplexed MAPK biosensor cells, MCF10As were infected with a lentiviral H2B-iRFP vector (Addgene) and sorted. We used gateway cloning to introduce ERK-KTR-mCer3, JNK-KTR-mRuby2, and p38-KTR-mClover into PGK pLenti DEST vectors (Addgene), infected and selected the H2B-iRFP MCF10As (Blasticidin 3 µg/ml and Hygromycin 10 μg/ml Corning). We isolated moderately expressing clones using cloning cylinders (EMD Millipore). For inducible cells, a gateway-ready reverse TET trans-activator (rtTA) plasmid was created by adding the rtTA with a 2A peptide to the Puromycin resistance gene in a CMV Puro DEST plasmid (Addgene) by gibson cloning (Gibson et al., 2009). Human coding sequences were acquired from either Addgene or the Thermo Ultimate ORF Collection, sequence-verified, and introduced in the rtTA CMV Puro DEST plasmid by gateway cloning(Campeau et al., 2009). These plasmids were used for lentivirus, and infected cells were selected with Puromycin (1 μg/ml, Sigma). Single-cell clones were then selected using cloning cylinders (EMD Millipore).

For inhibitor experiments, small molecules or antibodies and doxycycline were dissolved to a 10X working concentration in imaging media before addition. The final DMSO concentration did not exceed 0.15%. Inhibitors used include the ERK inhibitor Ulixertinib, the ASK inhibitor Selonsertinib, the MLK inhibitor URMC-099, the RAF inhibitor TAK-632, the MEKK inhibitor Ponatinib, the EGFR inhibitor Gefitinib, and the p38 inhibitor BIRB-796, all from Selleck Chemicals. The JNK inhibitor JNK-XVI (JNK-inh-8) and the COT inhibitor Cot-inhibitor-1 were obtained from MedChem Express. The p38 inhibitor SB-203580, and the TAK1 inhibitor 5Z-7-Oxozeaenol were obtained from Sigma.

The COT, TAK, and ZAK knockout cell lines were created using the CRISPR V2 Neo system (a gift from Dr. Andrew Holland) and specific gRNA oligos. MAPK biosensor cells were infected with lentivirus carrying these plasmids, selected with Neomycin (500 μg/ml, Sigma), and clonally expanded before western blot validation.





Live Imaging

Cells were plated at *2.710 \sigma 5 cells/well in fibronectin-coated (EMD Millipore) 96-well glass-bottom plates (Thermo Scientific or Cellvis) 48 hr before imaging. The following day, monolayers were serum-starved with 0.5% HS, phenol-red-free DMEM/F12 containing 1% Glutamax (Gibco). Monolayers were imaged using a Metamorph-controlled Nikon Eclipse Ti-E epifluorescence microscope with a 20x air objective and a Hamamatsu sCMOS camera. The multi-LED light source SpectraX (Lumencor) and the multiband dichroic mirrors DAPI/FITC/Cy3/Cy5 and CFP/YPF/mCherry (Chroma) were used for illumination and imaging without any spectral overlap. Temperature (37°C), humidity, and CO2 (5%) were maintained throughout all imaging using OKO Labs control units. Time-lapse images were captured at 5-minute intervals. Sample sizes were selected by attempting to capture at least 300 cells from each population. Key conditions from imaging experiments were performed at least twice, with one independent replicate presented in figures. All experiments have at least two technical replicates per independent experimental replicate.

Image Analysis and Quantification

Primary time-lapse images were subjected to flat-fielding and registration before further analysis. Tet-induction experiments were segmented and tracked as previously described (Aikin et al., 2020). All other imaging experiments were analyzed using python based neural net segmentation. Binary images where then imported into CellProfiler for measurement. As described in Aikin et al., the cytoring is determined as the area that projects out from the identified nuclei for a diameter of 4 pixels, unless in any area it encounters another cytoring, in which case it is segmented at the intersection. Intensity ratios were calculated as previously described (Regot et al., 2014). Single-cell traces were chosen by random plotting of distinct cells and selection of those that were tracked throughout the whole experiment. Peak counting was performed with software based on findPeaks and as previously described (Aikin et al., 2020).

Immunoblotting

Cells were plated to confluency in 6-well plastic cell culture plates and starved with 0.5% HS, DMEM/F12 overnight before specified treatment and lysate collection. Protein samples were collected in RIPA buffer (CST) with 1× HALT protease/phosphatase inhibitor (Thermo) and reduced in Laemlli SDS buffer (BioRad) with BME (Sigma). Protein was loaded onto 4-15% gradient polyacrylamide gels (Bio-Rad). After electrophoresis proteins were transferred to Trans-Blot nitrocellulose membranes (Bio-Rad, 1704159EDU). Blots were probed overnight at 4 °C with mouse MEK1/2 (CST 4694S), rabbit pMEK1/2 (CST 9154S), rabbit pMKK7 (Abcam ab4762), rabbit pMKK4 (CST 4514S), rabbit pMKK3/6 (CST9231), rabbit COT (Genetex GTX102711), TAK1 (SCBT), mouse anti-HSC70 (Santa Cruz Biotechnology), and IRDye donkey anti-rabbit 800 and goat anti-mouse 680 secondary antibodies (LiCor) before imaging. All images were acquired on an Odyssey Infrared Scanner (LiCor).

Cell Death Assay

To measure cell death, MCF10A cells were plated (27,000 cells per well) onto glass-bottom 96 well imaging plates (Thermo Fisher Scientific) and starved as described above. 24 hours later, the cells were incubated with 10 µM of CellEvent Caspase-3/7 Green Detection Reagent (Thermo Fisher Scientific, C10423) and imaged as previously described (Wu et al., 2020) following treatments as stated.

Experimental replicates and statistical power

All live imaging experiments have two technical replicates that are combined and represented in the main figures and are representative of at least three independent experimental replicates unless otherwise stated. All fixed imaging experiments have ten technical replicates and at least two independent experimental replicates. All western blots have at least three independent replicates. To overcome issues with high power, we first quantified p-values of large data sets using 2-way Anova and then applied a Bonferroni correction ('ns', not significant, *p<0.05, **p<0.01, ***p<0.001).